Astron. Nachr. / AN **328**, No. 3/4, 215 – 222 (2007) / **DOI** 10.1002/asna.200610722

Measuring helioseismic travel times

M. Roth[1,⋆], **L. Gizon**[1], and **J.G. Beck**[2]

[1] Max-Planck-Institut für Sonnensystemforschung, 37191 Katlenburg-Lindau, Germany
[2] W.W. Hansen Experimental Physics Laboratory, Stanford University, CA 94305, USA

Received 2006 Dec 21, accepted 2007 Jan 2
Published online 2007 Feb 28

Key words Sun: helioseismology – methods: data analysis

In time-distance helioseismology wave travel times are measured from the cross-correlation between Doppler velocities recorded at any two locations on the solar surface. We compare two different methods to extract the travel times from the noisy cross-correlation functions. The first method consists of fitting a 5-parameter analytic function to the cross-correlation to obtain the phase travel time. The second method consists of linearizing the distance between the observed cross-correlation and a sliding reference cross-correlation (the only parameter is the travel time). We find that the one-parameter fits are more robust with respect to noise. Using SOHO data from the MDI Structure Program for the years 1996–2003, we study in detail the statistical properties of the noise associated with the travel-time measurements for the two different fitting methods.

1 Introduction

Time-distance helioseismology was introduced by Duvall et al. (1993). It consists of analysing the travel times of acoustic wave packets that propagate through the Sun. Inhomogeneities, like flows or sound speed anomalies, affect the travel times of solar waves. The travel times are estimated by cross-correlating the oscillation signal between any two locations on the solar surface. A critical step in the data analysis is to extract the acoustic wave travel times from the cross-correlation function.

We implement two measurement techniques and compare them for robustness to solar noise. The first method consists of fitting a 5-parameter analytic function to the cross-correlation to obtain the phase travel time (Kosovichev & Duvall 1997). The second method consists of linearizing the distance between the observed cross-correlation and a sliding reference cross-correlation, where the only parameter is the travel time (Gizon & Birch 2004). This last method is motivated by studies in geophysics (Zhao & Jordan 1998).

Here we use a set of velocity maps recorded every minute by the Michelson Doppler Imager (MDI) during the period 1996–2003 (SOHO/MDI Structure Program, Scherrer et al. 1995). This long time series of observations enables us to study in detail the statistical properties of the noise associated with the travel-time measurements for the two different fitting methods.

⋆ Corresponding author: roth@mps.mpg.de

2 Observations

The data consist of medium-resolution MDI Dopplergrams. The data reduction has been described by Giles (2000). Images were grouped into 72-hour periods for de-trending of solar rotation and supergranulation. Regions, spanning 100° in latitude and longitude, were tracked at the Carrington rotation rate for the 72-hour period. These tracked regions were remapped into a cylindrical equal-area projection and stacked into a data cube. In this projection the pixels are equally spaced in longitude and in sine latitude; thus pixels in a given column all have the same longitude and pixels in a row all have the same latitude. The scale of this projection matches the angular resolution of the input images at disk center, consequently the image is oversampled at other locations. Subsequent processing included applying a high-pass filter at 1.7 mHz to remove the supergranulation signal. We then apply a filter to the data to remove the f-mode signal.

Temporal cross-correlations $C(t)$ were obtained using code developed by Giles (2000) using pairs of points separated in latitude. For pixels aligned north-south the separation ranged from $\Delta = 3^\circ$ to 45°, and $\Delta = 3^\circ$ to 19.2° for east-west. To enhance the signal, the resulting cross-correlations were averaged spatially according to the quadrant averaging scheme shown in Fig. 1. Then, these cross-correlations were averaged over all longitudes and saved to files for each nominal latitude λ.

The cross-correlations are stored in `FITS` format. The header parameters associated with each file are described in the Appendix and in part by Giles (2000). The files are organized as follows: within each file each row contains $2N + 4$ elements. The first element is the mean travel distance. The second element is the total number of pairs of

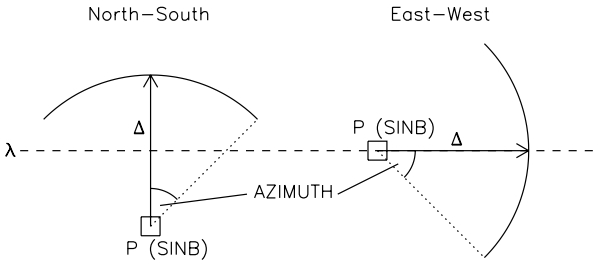

Fig. 1 The geometry for obtaining either the cross-correlations for north-south (*left*) or east-west (*right*) propagating wave packets. The oscillation signal observed at pixel P is correlated with the oscillation signal observed at pixels on the arc. The angular distance between the pixel P and the pixels on the arc is Δ. Then, these cross-correlations are averaged. After further averaging over all longitudes the cross-correlations are saved to FITS files for the latitude given by λ. The FITS files contain header parameters: the latitude of pixel P is given by SINB, the angular width of the arc is given by AZIMUTH.

image pixels which have been used to compute the cross correlation. The third element is the average deviation in degrees from the target direction for propagation between the pairs of pixels. The maximum deviation from the target direction is given by the header parameter AZIMUTH. The remaining elements in the row are the cross-correlation from time lag $-N$ to time lag $+N$ in minutes. The columns within each file contain $(\texttt{DMAX} - \texttt{DMIN})/\texttt{DRANGE} + 1$ elements, with DMIN the minimum travel distance; DMAX the maximum travel distance, and DRANGE the sampling of the distance axis in degrees.

Figure 2 displays north-south cross-covariances averaged over the period from May to July 1996 as a function of time lag and distance. Several ridges are visible in this plot. They correspond to the different bounces of the wave packets at the surface before reaching the distance Δ. The first ridge with smallest time lag corresponds to the direct arrival of a wave packet. The other ridges correspond to wave packets that bounce off the surface once or more before reaching the distance Δ. The amplitude of the cross-covariance fades away at large distances Δ due to the geometrical spread of the wave energy and wave damping. The signal-to-noise ratio at large distances is less.

3 Measuring travel times

We describe the two fitting techniques that are used to measure the travel times from the cross-covariances. We fit separately the first bounce and second bounce travel times. The fitting ranges are indicated in Fig. 2 (bottom).

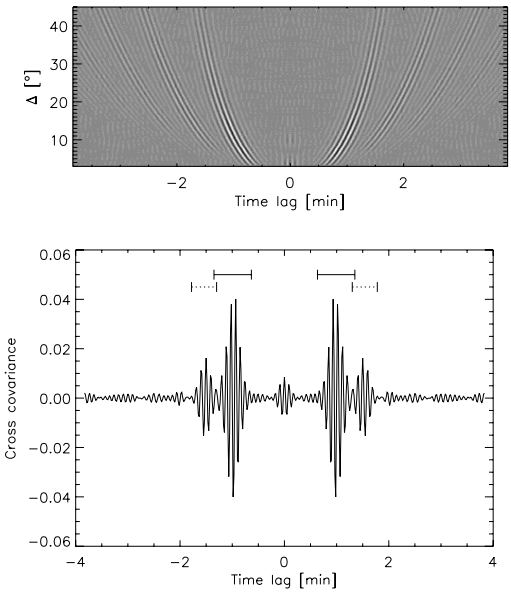

Fig. 2 *Top*: averaged cross-covariance as a function of time lag and distance Δ. The average was carried out for North-South data at the equator over 90 days from May–July 1996. *Bottom*: Cut through the top diagram at $\Delta = 10.5°$. The solid and dotted lines mark the fit ranges for the first and second bounces, respectively.

3.1 Gabor wavelet fitting

For each bounce, the cross-covariance can be approximated by a Gabor wavelet (Kosovichev & Duvall 1997)

$$\hat{C}(t) = A^2 \cos(\omega_0(t + t_\mathrm{p})) \exp\left(-\frac{(t - t_\mathrm{g})^2}{2\sigma^2}\right), \qquad (1)$$

where A^2 is the amplitude, ω_0 the frequency, t_p the phase travel time, t_g the group travel time and σ^2 the width of the Gaussian envelope. The group travel time t_g is given by the time lag of the peak of the envelope. The phase travel time t_p is defined as the modulo $2\pi/\omega_0$. In general t_p can be determined with higher accuracy than t_g. Note that the two branches of the cross-covariance, $C(t > 0)$ and $C(t < 0)$, are fitted separately. The corresponding phase travel times are denoted as t_{p+} for $C(t > 0)$ and t_{p-} for $C(t < 0)$.

In order to fit individual cross-covariances initial guesses for all the parameters are needed. Here we describe in detail the procedure that we use to determine these guesses. We use the long-term average cross-covariance shown in Fig. 2 to obtain initial guesses. As shown in Fig. 3 the guess for t_p is important because of the non-uniqueness of t_p. The guess for t_p is obtained iteratively.

As a first step all phase travel-time measurements that are more than $2\pi/\omega_0$ away from the initial guess are removed. Secondly, the remaining measurements of t_p are used to find the coefficients of a fifth-order polynomial to the phase time-distance relation (Chou & Duvall 2000). Thirdly, this fifth-order polynomial together with the original guesses for A^2, σ^2, ω_0 and t_g are used as new guesses

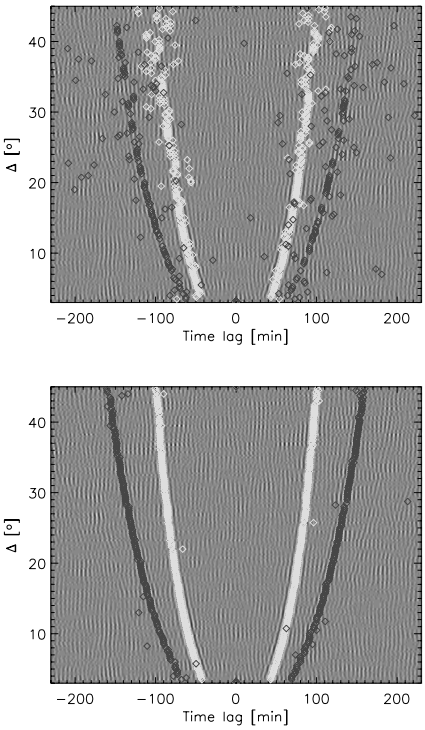

Fig. 3 Time-distance diagram with phase travel-time measurements $t_{\rm ph}$ for the first (light grey) and second (dark grey) bounce in north-south data; $T = 72$ h, $\lambda = 0^\circ$. *Top*: Phase travel-time measurements obtained by Gabor-wavelet fits with a rough guess for $t_{\rm ph}$. *Bottom*: Phase travel-time measurements obtained by Gabor-wavelet fits with a guess for $t_{\rm ph}$ obtained after five steps of iterating the relation $t_{\rm ph}(\Delta)$ by fifth-order polynomials.

for a further iteration of the Gabor-wavelet fit. The procedure is repeated until the guesses converge. Figure 3 (bottom) shows phase travel-time measurements for the first and second bounce after five iterations.

Once final guesses have been determined, the individual $T = 72$ h cross-covariances can be fitted one at a time (see Fig. 4 for an example). Outliers in the $t_{\rm p}$ measurements may occur. By definition we call outliers measurements that lie 3σ away from the mean. We investigate the statistics of the travel-time measurements in Sect. 4.

3.2 One-parameter fit

Another approach of determining one-way travel-time measurements is to compare the observed cross-covariance with a sliding reference model $C_{\rm ref}$. The reference cross-covariances are obtained by averaging the cross-covariance functions over 90 days (cf. Fig. 2). In order to reduce the imprint of long lived flows these averages are then symmetrized with respect to time lag $t = 0$.

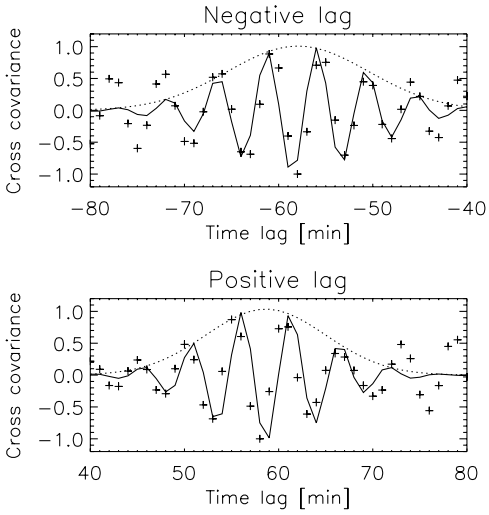

Fig. 4 Gabor-wavelet fits (solid lines) to the cross-covariance (crosses) for north-south data, $T = 72$ h, $\lambda = 0^\circ$, $\Delta = 10.5^\circ$. Shown are the fit results for the negative (*top*) and positive (*bottom*) time lags. The dotted lines give the envelope of the fitted wavelet.

The reference cross-covariance is shifted in time until it best resembles the data (Gizon & Birch 2002). The travel time is defined by:

$$\tau_\pm = \frac{\sum_i \mp f(\pm t_i)\dot{C}_{\rm ref}(t_i)[C(t_i) - C_{\rm ref}(t_i)]}{\sum_i f(\pm t_i)[\dot{C}_{\rm ref}(t_i)]^2}\,, \qquad (2)$$

where $\dot{C}_{\rm ref}$ is the time derivative of the reference cross-covariance. Equation (2) is the result of applying a linearization procedure (Gizon & Birch 2004).

The window function $f(t)$ selects the ridge of interest in the time-distance diagram. We use a boxcar function centered on the first or second ridge, respectively. We denote by τ_+ the travel time for waves that move away from the starting location and by τ_- the travel time for waves that move in the opposite direction. For each λ and Δ we obtain a measurement of τ_+ and τ_-. We note, in this procedure no fitting algorithm is involved. Therefore, convergence problems cannot occur. A travel-time measurement is always obtained.

4 Comparison of the two travel-time measurement techniques

Here we consider the travel-time differences. In the case of Gabor-wavelet fits these are given by $t_{p+} - t_{p-}$. In the case of the one-parameter fits these are $\tau_+ - \tau_-$. We compare the two measurement techniques. Both methods are affected by noise in the cross-covariances. We study the sensitivity of the two methods to this noise.

Figure 5 shows travel-time shifts measured at the equator as a function of distance in north-south data. In general the two methods agree well. However, the Gabor-wavelet

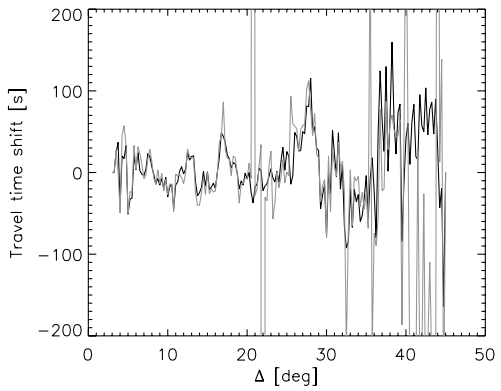

Fig. 5 Travel-time differences at the equator for north-south data as a function of distance Δ. Shown are results of the two measurement techniques Gabor-wavelet fit (grey) and one-parameter fit (black). Both measurements are obtained from the same cross correlations and the observation time is $T = 72$ h.

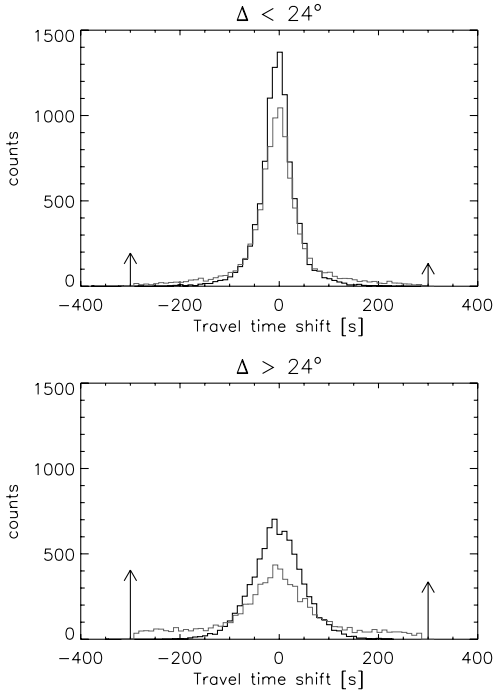

Fig. 6 Histograms for travel-time shifts measured by the Gabor-wavelet fit (grey) and the one-parameter fit (black) applied to north-south data; $T = 72$ h. *Top*: Measurements for distances lower than 24°. The total number of measurements is 9667. *Bottom*: Measurements for distances larger than 24°. The total number of measurements is 8036. In both cases the number of outliers produced by the Gabor-wavelet fit are indicated by arrows at the bins -300 s and 300 s, resp. The total number of outliers is 327 for $\Delta < 24^\circ$ and 741 for $\Delta > 24^\circ$.

fitting produces outliers, even more frequently at large distances where the signal-to-noise ratio is worse. There the one-parameter fit still delivers results. We compare the distributions of travel-time shifts for all latitudes λ; once for distances Δ smaller than 24° and once for distances Δ larger than 24° for one observing period of length $T = 72$ h, cf. Fig. 6. The binning in the histograms is 10 s. There are 9667 travel-time measurements for $\Delta < 24^\circ$ and 8036 measurements for $\Delta > 24^\circ$. We find in general for both methods a broader distribution for the larger distances. This is expected due to the fading signal with greater distances (cf. Fig. 2, top). Comparing the two measurement techniques the distribution for the Gabor-wavelet fit is always broader than the distribution for the one-parameter fit. The distribution of the one-parameter fits is Gaussian (Gizon & Birch 2004), whereas the distribution of the Gabor-wavelet fits has flat tails which shows that the distribution is not Gaussian. All the measurements in the flat tails are suspected to be wrong. We note, that the Gabor-wavelet fit produces a non-negligible amount of outliers. The number of outliers are indicated by arrows in the histograms. The relative number of outliers for $\Delta < 24^\circ$ is 3.3%. The relative number of outliers for $\Delta > 24^\circ$ is 9.2%. There are no outliers with the one-parameter fit.

A further comparison is carried out by correlating the results of the two methods. For the whole time series all travel-time shifts are measured for each latitude λ and distance Δ. This results in two time series of travel-time shifts for each λ and Δ which are correlated. Figure 7 displays the correlation between the obtained travel-time shifts as a function of distance and latitude. The correlation between the two methods for first bounce measurements is good. At distances between 5° and 15° and in regions $\pm 20^\circ$ around the equator the correlation coefficient reaches values larger than 0.9. The correlation drops towards larger and smaller distances and towards higher latitudes.

For second bounce measurements the correlation is in general lower. At distances between 10° and 15° and $\pm 10^\circ$ around the equator the correlation coefficient reaches the highest values (> 0.8). In all other regions the correlation coefficient is lower than 0.6 and drops fast to larger and smaller distances and to higher latitudes. The loss of correlation at smaller and greater distances and at higher latitudes is mainly due to a larger scatter in the measured travel-time shifts and the more outliers in the Gabor-wavelet fit.

The noise in the travel-time measurements goes down as T increases. This is what we show in Fig. 8. We subdivided our time series of north-south and east-west cross-covariances into sub-samples with durations of 3, 30, 90, 360, and 1200 days. For each sample the cross-covariances were averaged. As the time series covers 2613 days we therefore obtained 871, 87, 29, 7, and 2 travel-time measurements for each λ and Δ. From these sets of measurements we determine the respective standard deviations. The observed standard deviations scale with $1/\sqrt{T}$ for all latitudes λ and all distances Δ. This dependence on T has been demonstrated theoretically in case of the one-parameter fit (Gizon & Birch 2004), and we have just shown that it also applies in the case of the Gabor-wavelet fit.

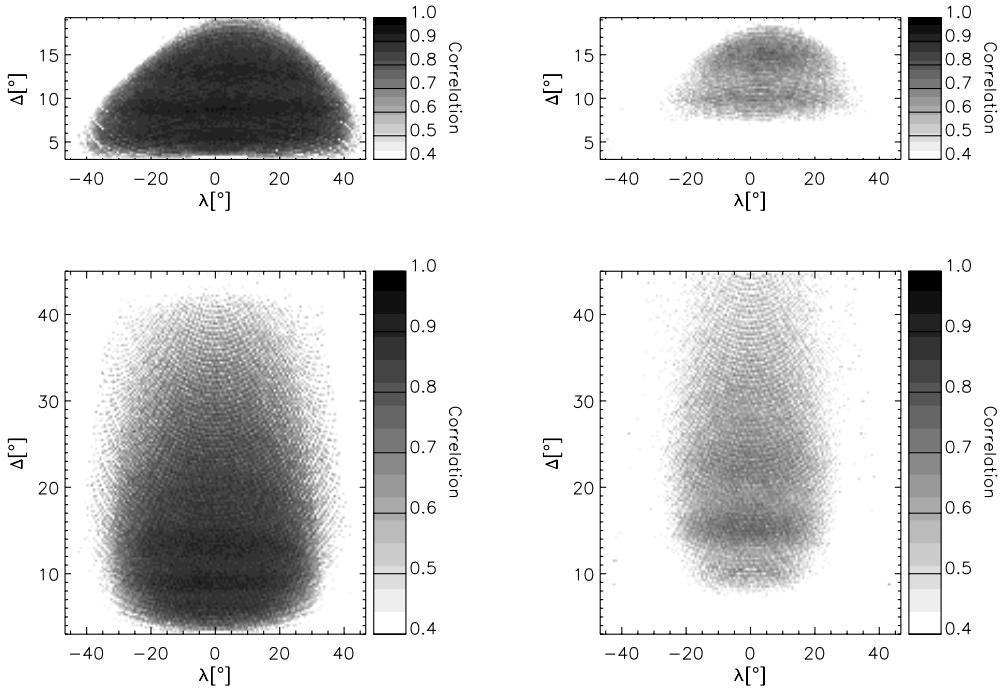

Fig. 7 Correlation between travel-time shifts obtained by the two measurement methods as a function of latitude λ and distance Δ. *Top row*: east-west data, *bottom row*: north-south data. *Left column*: correlations for the first-bounce measurements; *right column*: correlations for the second-bounce measurements. The color scale saturates below a correlation coefficient of 0.4. The observing period was $T = 72$ h.

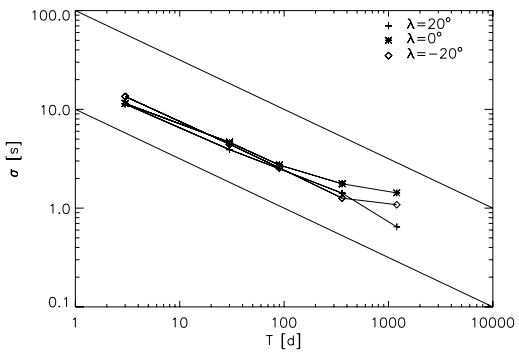

Fig. 8 Standard deviations σ of the observed p-mode travel times for the three latitudes $\lambda = -20^\circ$, 0°, and 20° as a function of observing time T. The measurements where obtained for an angular distance of $\Delta = 10^\circ$ by Gabor-wavelet fitting. The solid lines indicate the $T^{-1/2}$ dependence. The same T dependence is found for the one-parameter fit.

The signal-to-noise ratio in the cross-covariances varies as a function of λ and Δ. This is mirrored in the travel-time measurements. Their standard deviation is also a function of λ and Δ (cf., Fig. 9). The standard deviation is lowest $\pm 20^\circ$ around the equator, i.e. $\lambda = 0^\circ$, and at distances around $\Delta = 10^\circ$. Towards higher latitudes and towards smaller and greater distances the noise is stronger. This result is comparable with the results obtained by Giles (2000). In general, the one-parameter fit results in a lower variance of the measurements.

The two measurement methods agree well. However, the one-parameter fit is more robust and has a lower variance. Therefore, we pick the results from the one-parameter fit to study the noise-covariance matrix. The noise covariance matrix is useful when carrying out inversions (Jackiewicz et al. 2007). It is obtained by cross-correlating the time series of travel-time shifts.

Figure 10 shows the noise correlation matrix $\mathrm{Cor}(\lambda, \Delta; \lambda', \Delta')$ for travel-time shifts. The plots show the two cases $\lambda = \lambda' = 0^\circ$ and $\lambda' = 0^\circ, \Delta' = 8^\circ$ for the north-south and east-west data. In both the north-south and the east-west data the correlations fall off very rapidly away from the diagonal in the first case or away from the location $\lambda = 0^\circ, \Delta = 8^\circ$ in the second case. The slightly different structure of the north-south and east-west correlation matrix is due to the different geometries when obtaining the cross-covariances.

For the case $\mathrm{Cor}(\lambda = 0^\circ, \Delta; \lambda' = 0^\circ, \Delta')$ in the north-south data, there is only one sidelobe at distances 2° off the diagonal with amplitude of about 0.2. In the east-west data there are two sidelobes at distances 2°, and 4° off the diagonal with amplitudes below 0.2. For the case $\mathrm{Cor}(\lambda, \Delta; \lambda' = 0^\circ, \Delta' = 8^\circ)$ the north-south data show a

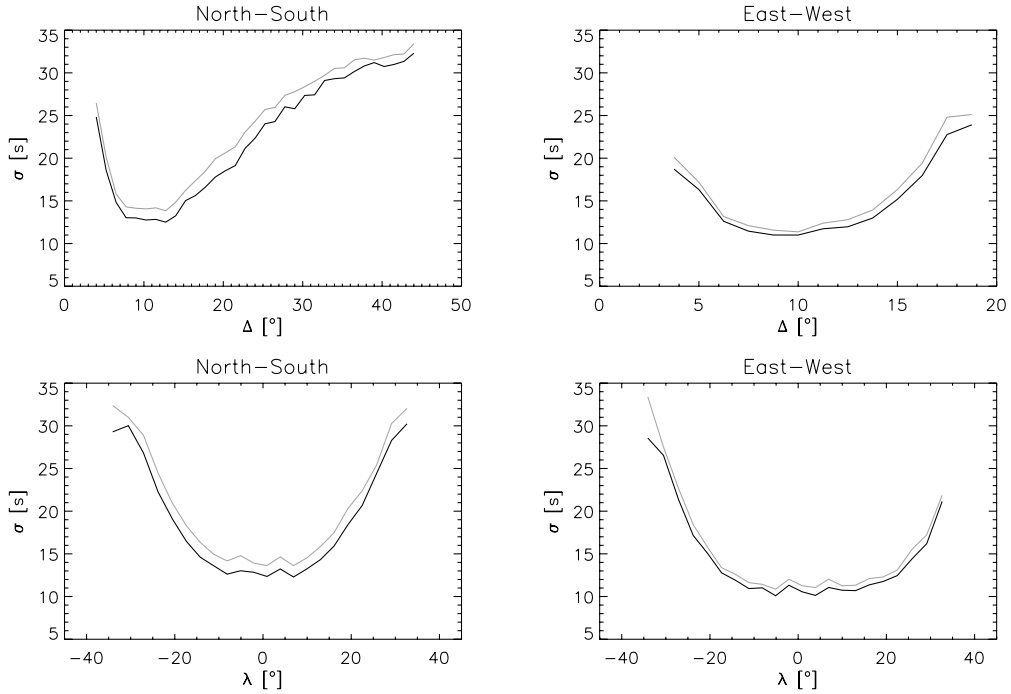

Fig. 9 Standard deviation of north-south (*left*) and east-west (*right*) travel-time differences as a function of distance at the equator (*top*) and as a function of latitude at distance 10° (*bottom*). The travel-time differences were obtained using a Gabor-wavelet fit (grey) and the one-parameter fit (black) for $T = 72$ h. Outliers in the Gabor-wavelet fits were removed. The results were binned over 2.4° on the axes.

well confined peak at the location $\lambda = 0^\circ, \Delta = 8^\circ$. This peak has a width of 0.3° in λ and 0.5° in Δ. There exists a strip ranging in λ between $\pm 15^\circ$ and in Δ between $\pm 0.5^\circ$ around the main peak with a correlation of about 0.1. Additionally, 0.5° wide peaks with correlation of about -0.2 are located $\pm 1^\circ$ in Δ-direction away from the target location. They correspond to the sidelobes of the case $\mathrm{Cor}(\lambda = 0^\circ, \Delta; \lambda' = 0^\circ, \Delta')$. The east-west data do not exhibit a wide strip in the noise correlation matrix. There exist only additional peaks which correspond to the sidelobes of the case $\mathrm{Cor}(\lambda = 0^\circ, \Delta; \lambda' = 0^\circ, \Delta')$. The locations of the peaks differ slightly from $\lambda = 0^\circ$. The width of these peaks in λ is about 2°.

5 Conclusions

We analysed cross-covariances covering the years 1996–2003, and computed from MDI Doppler velocity maps. We measure helioseismic travel-times by two different techniques. One method was the traditional method of fitting Gabor wavelets to obtain the phase time (Kosovichev & Duvall 1997), the other method was a one-parameter fit (Gizon & Birch 2004). We compared the two travel-time measurements. In general both methods agree well. The definition of travel time according to Gizon & Birch (2004) is robust to noise, because no fitting algorithm is involved. The distribution of measurements is Gaussian in that case. The Gabor-wavelet fitting is not as robust and provides a non-Gaussian distribution of travel-time measurements.

The variance of the measurements is a function of latitude and distance with a minimum at distances around $\Delta = 10^\circ$ and latitudes $\pm 20^\circ$ around the equator. This finding agrees with the results obtained by Giles (2000). After removing the outliers returned by the Gabor-wavelet fits we find that the noise in the travel times is similar for both measurement methods. The standard deviation of the noise for both fitting methods decreases with observation time T as $T^{-1/2}$.

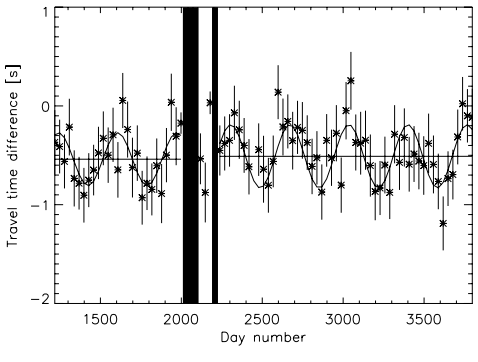

Fig. 11 North-south travel-time shifts averaged over $\lambda = \pm 10^\circ$ around the equator as a function of time. Plotted are 30 day averages and error bars. Travel-time measurements were obtained by the one-parameter fit. The 1 yr periodicity is attributed to an error in the determination of the direction of the solar rotation axis (Beck & Giles 2000; Beck 2005).

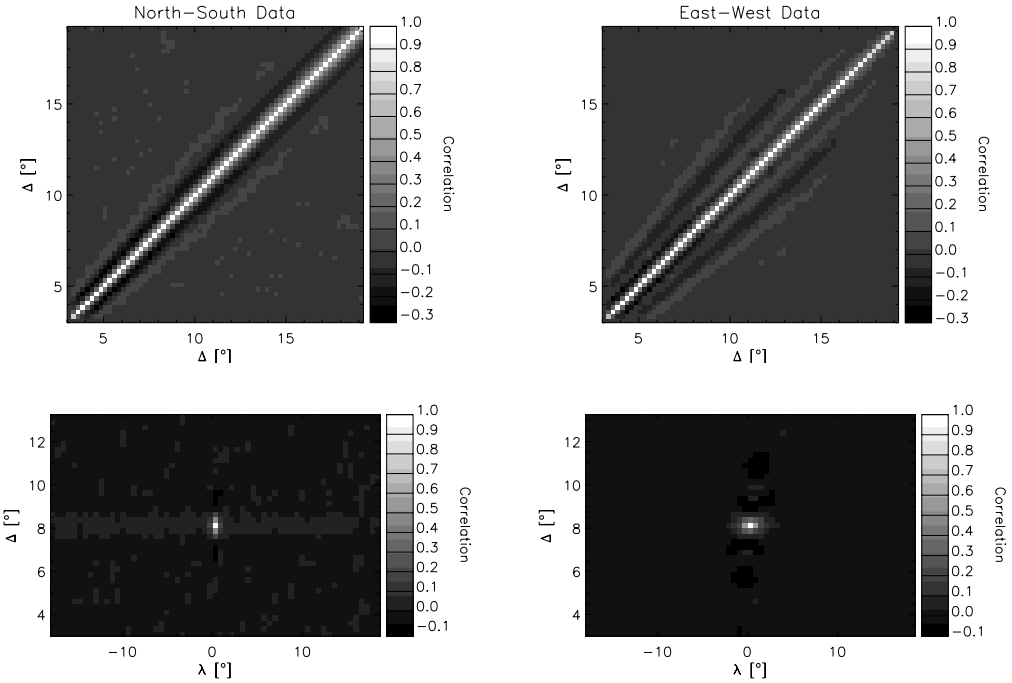

Fig. 10 The noise correlation matrix $\mathrm{Cor}(\lambda, \Delta; \lambda', \Delta')$ for north-south (*left*) and east-west travel-time shifts (*right*). The top row is for $\lambda = \lambda' = 0^\circ$, the bottom row is for $\lambda' = 0^\circ, \Delta' = 8^\circ$. Note the different scales on the axes.

To illustrate the fact that the one-parameter fit reproduces previously known results, we show in Fig. 11 the temporal variation of the travel times near the equator. This plot reveals a one-year periodicity in the north-south travel-time differences, which was first pointed out by Giles (2000) and attributed to an error in the determination of the direction of the rotation axis of the Sun. This agreement for such a small effect is encouraging.

We did not study whether the two methods are unbiased. Large travel-time shifts as they occur in sunspots may introduce such biases. We do not, however, expect phase travel-time shifts in excess of $2\pi/\omega_0$ given the low spatial resolution of the MDI Structure Program data and an observation duration of $T = 72$ h.

The travel-times discussed in this paper need further processing in order to infer localized information in the solar interior. One advantage of the one-parameter fits is that travel-time sensitivity kernels already exist for such measurements (Birch et al. 2004; Birch & Gizon 2007). We note that an inversion of the travel-time measurements requires some knowledge of the noise covariance matrix discussed in Sect. 4. The off-diagonal elements of the noise covariance matrix have been shown here to be negligible about 2° away from diagonal (Fig. 10).

Acknowledgements. The code that generated the cross-correlations was written by Peter Giles and is described in his PhD thesis (Giles 2000). We thank T.L. Duvall for useful discussions. M. Roth acknowledges support from HELAS to participate at the workshop "Roadmap for European local helioseismology" in Nice. The European Helio- and Asteroseismology Network (HELAS) is funded by the European Union's Sixth Framework Programme.

References

Beck, J.G., Gizon, L., Duvall, T.L., Jr.: 2002, ApJ 575, L47
Beck, J.G., Giles, P.: 2005, ApJ 621, L153
Birch, A.C., Kosovichev, A.G., Duvall, T.L., Jr.: 2004, ApJ 608, 580
Birch, A.C., Gizon, L.: 2007, AN, this volume
Chou, D.-Y., Duvall, T.L., Jr.: 2000, ApJ 533, 568
Duvall, T.L., Jr., Jefferies, S.M., Harvey, J.W., Osaki, Y., Pomerantz, M.A.: 1993, Nature 362, 430
Giles, P.: 2000, Thesis, Stanford Univ.
Gizon, L., Birch, A.C.: 2002, ApJ 571, 966
Gizon, L., Birch, A.C.: 2004, ApJ 614, 472
Jackiewicz, J., Gizon, L., Birch, A.C., Thompson, M.J.: 2007, AN, this volume
Kosovichev, A., Duvall, T.L., Jr.: 1997, in: F.P. Pijpers et al. (eds.), *SCORe '96: Solar Convection and Oscillations and Their Relationship*, p. 241
Scherrer, P.H., et al.: 1995, SoPh 162, 129
Zhao, L., Jordan, T.H.: 1998, GeoJI 133, 683

A Header parameters of the FITS files of the MDI cross-covariances

The code that generated the cross-correlations was written by Peter Giles and is described in his PhD thesis (Giles 2000). Table A1 gives the complete list of the parameters that are contained in the headers of the cross-correlation files that are generated by his code and that are archived at Stanford University in the SOI database.

Table A1 Keywords in the header of the FITS files that contain the MDI cross-covariances.

Keywords from Track_region module which produces the tracked data cubes:	
T_FIRST / T_LAST	The time of the first/last MDI VWV images in tracked data cube.
MAP_PROJ	The type of map projection used in data cube (cylinder-equal area is the type used for this work.
MAPSCALE	The resolution of the tracked data in arc-secs/ pixel at disk center.
TRACK_A0, TRACK_A2, and TRACK_A4	Coefficients for the differential rotation used for tracking.
MERID_V	The rate of meridional velocity for tracking (not used).
HG_LAT / HG_LONG	The center of the tracked region in heliographic coordinates (long/lat).
BACKGRND	The name of a background image which is subtracted from all images before tracking.
Keywords from Xcorr – the module which produces the cross-correlations from the tracked regions:	
DIRECT	This parameter determines how the pairs of points are chosen for cross-correlation. If the direction is "N", then the pairs of points have the same (or similar) longitudes. Otherwise, the pairs of points have the same (or similar) latitudes.
DMIN	The minimum distance to be computed, in degrees. The default is zero (the cross-correlation for two points separated by zero distance is the autocorrelation).
DMAX	The maximum distance to be computed, in degrees. The default is the largest distance that would be possible to compute if AZIMUTH was set to zero, given the size of the input data cube.
DTMAX	The maximum correlation time ("lag") to be included in the output, in number of time intervals. The default is to make an output file that is as long as the input file, plus one. This is probably not usually what is wanted. In general, there is little use in including lags of more than a few hours.
DTMIN	The minimum correlation time ("lag") to be included in the output, in number of time intervals. The default is to make an output file that is as long as the input file, plus one. This is probably not usually what is wanted. In general, there is little use in including lags of more than a few hours.
T_STEP	The time between steps in the lag in the output correlations (usually 60 s).
DRANGE	The size of the output distance bins. The size of the output file is reduced and the noise in the cross-correlations is also reduced. Cross-correlations for similar distances are averaged together. This reduces the output and increases the signal-to-noise in the resulting cross-correlations. The units of DRANGE are degrees.
AZIMUTH	This parameter determines the maximum deviation from the target direction. The default is 0.0, meaning only cross-correlate for points on the same line of longitude (or parallel of latitude if DIRECTION = "W"). Any non-zero value for AZIMUTH results in additional cross-correlations being computed. AZIMUTH = 1.0, for example, will include all points which have an azimuth of ± 1.0 degrees, measured from sun north. The idea is to improve the signal-to-noise by including additional cross-correlations for pairs of points that have "almost" the right relative positions.
FPASS	The cutoff frequency for the default high-pass filter, in Hz. The default corresponds to a period of about 9.8 minutes; the filter is designed to remove the low-frequency noise due to convective motions.
FWIDTH	The width of the frequency filter "roll-off," as a fraction of the cutoff frequency FPASS. The high-pass filter has a Gaussian roll-off of width FWIDTH * FPASS and peaks at FPASS. Above FPASS the filter is constant. Setting FWIDTH = 0 results in a square cutoff.
FMODE	(flag) F-mode filter: Filter out the f-mode (0), or not (1).
KCORRECT	(flag) K-correct or flatten the spatial frequency response by boosting the high-k signal, and correct for instrumental astigmatism. Note that these filters are designed for the MDI instrument and are probably not appropriate for other instruments.
SORT	(flag) Sort the output file by travel distance. The default (0) is to do this. If SORT = 1 is specified then the output may not be a very nice-looking time-distance diagram. Note that specifying DRANGE = 0(!) implies SORT = 0.
MORE	(flag) This option causes separate FITS files to be output, containing the list of all distance, averaging, and direction information. This is ignored if DRANGE = 0.0 (the default). It is intended to be used to give the additional information about the distance bins when averaging is used (DRANGE > 0.0).
PAD	(flag) When this flag is set, the time series in each pixel is padded with DTMAX zeros before the processing. This is of course necessary to avoid contamination from edge effects in the cross correlation. However, the effect of the low-pass frequency filter (see FPASS, FWIDTH) is to put a region of zero data at one end, which corrects the problem already. The default is not to do it.
VPFILT	(flag) When this flag is set, a phase speed filter is applied to the data.
DIRFILT	(flag) filter for target direction (i.e. either north-south or east-west)
TOL	The allowable percentage of off-disk pixels.
LONGDIVS, LATDIVS, and TIMEDIVS	Dimensions of data cube in longitude, in latitude, and in time.
SINBDELT	Resolution of the input data cube in sine latitude.

